


Article

Shear Strength Estimation of Reinforced Concrete Deep Beams Using a Novel Hybrid Metaheuristic Optimized SVR Models

Mosbeh R. Kaloop^{1,2,3}, Bishwajit Roy⁴, Kuldeep Chaurasia⁴, Sean-Mi Kim¹, Hee-Myung Jang¹, Jong-Wan Hu^{1,2,*}  and Basem S. Abdelwahed⁵

¹ Department of Civil and Environmental Engineering, Incheon National University, Incheon 22012, Korea; mosbeh@mans.edu.eg (M.R.K.); mook@hdec.co.kr (S.-M.K.); jhm924@kistep.re.kr (H.-M.J.)

² Incheon Disaster Prevention Research Center, Incheon National University, Incheon 22012, Korea

³ Public Works and Civil Engineering Department, Mansoura University, Mansoura 35516, Egypt

⁴ School of Computer Science Engineering and Technology, Bennett University, Greater Noida 201310, India; bishwajit.cse15@nitp.ac.in (B.R.); kchaurasia.nitb@gmail.com (K.C.)

⁵ Structural Engineering Department, Mansoura University, Mansoura 35516, Egypt; bs_hadi@mans.edu.eg

* Correspondence: jongp24@inu.ac.kr

Abstract: This study looks to propose a hybrid soft computing approach that can be used to accurately estimate the shear strength of reinforced concrete (RC) deep beams. Support vector regression (SVR) is integrated with three novel metaheuristic optimization algorithms: African Vultures optimization algorithm (AVOA), particle swarm optimization (PSO), and Harris Hawks optimization (HHO). The proposed models, SVR-AVOA, -PSO, and -HHO, are designed and compared to reference existing models. Multi variables are used and evaluated to model and evaluate the deep beam's shear strength, and the sensitivity of the selected variables in modeling the shear strength is assessed. The results indicate that the SVR-AVOA outperforms other proposed and existing models for the shear strength prediction. The mean absolute error of SVR-AVOA, SVR-PSO, and SVR-HHO are 43.17 kN, 44.09 kN, and 106.95 kN, respectively. The SVR-AVOA can be used as a soft computing technique to estimate the shear strength of the RC deep beam with a maximum error of $\pm 3.39\%$. Furthermore, the sensitivity analysis shows that the deep beam's key parameters (shear span to depth ratio, web reinforcement's yield strength, concrete compressive strength, stirrups spacing, and the main longitudinal bars reinforcement ratio) are efficiently impacted in the shear strength detection of RC deep beam.

Keywords: reinforced concrete; deep beam; shear strength; support vector regression; metaheuristic optimization



check for updates

Citation: Kaloop, M.R.; Roy, B.; Chaurasia, K.; Kim, S.-M.; Jang, H.-M.; Hu, J.-W.; Abdelwahed, B.S. Shear Strength Estimation of Reinforced Concrete Deep Beams Using a Novel Hybrid Metaheuristic Optimized SVR Models. *Sustainability* **2022**, *14*, 5238. <https://doi.org/10.3390/su14095238>

Academic Editors: Chiara Bedon, Maged A. Youssef, Mislav Stepinac, Marco Fasan and Ajitanshu Vedrtnam

Received: 22 March 2022

Accepted: 20 April 2022

Published: 26 April 2022

Publisher's Note: MDPI stays neutral with regard to jurisdictional claims in published maps and institutional affiliations.



Copyright: © 2022 by the authors. Licensee MDPI, Basel, Switzerland. This article is an open access article distributed under the terms and conditions of the Creative Commons Attribution (CC BY) license (<https://creativecommons.org/licenses/by/4.0/>).

1. Introduction

In many high-rise reinforced concrete (RC) buildings, as the use of areas is changed from one story to another, some columns in the upper stories are not permitted to reach the foundation. To solve this conflict, transfer girders with a considerable thickness named deep beams are required [1,2]. Furthermore, deep beams are used in many other critical structures and play a significant role in delivering heavy loads to the bearing elements [2,3]. Deep beams have high flexural stiffness, and the shear diagonal failure is the predominant mechanism as the loads are mainly transferred from their action points to the supports locations through a direct diagonal strut [1–4]. Concrete compressive strength, the provided top/bottom reinforcements, and web reinforcements in terms of amount and spacing all form the shear resistance of these deep beams [1,2,4,5]. In literature, plenty of analytical and numerical studies have been focused on the ultimate shear strength assessment of such beams with large depths compared to their spans [2,3,6–9]. Unavoidable discrepancies were found with the implementation of both analytical/numerical methods compared to the experimental results [4]. This study aims to propose a novel soft computing approach

that can be used to predict an accurate shear strength of RC deep beams based on a wide range of test results collected from different experimental studies.

Many researchers have used different regression methods to estimate the shear strength of RC deep beams [8,10]. Recently, soft computing techniques have been proposed and improved the prediction techniques of shear strength of beams [3,7,11–15]. A conventional artificial neural network (ANN) was applied to estimate the shear strength of the RC deep beam, and the accuracy of the designed model was high [7]. The ultimate shear strength of the RC deep beam was also estimated using ANN and compared to different building codes, and the proposed model provided an accurate prediction of shear capacity [6]. ANN, adaptive network-based fuzzy inference system (ANFIS), and group method of data handling (GMDH) approaches were used in predicting the shear strength of RC beam-column joints, and the performance of these models was high at a different range of shear strength [15]. A probabilistic model was applied to estimate the shear strength of beams, and the determination of shear strength was shown to be accurate [14]. Integrated genetic programming and simulated annealing (GSA) outperformed American concrete institute (ACI) and Canadian standard association (CSA) codes in modeling the shear strength of RC deep beams [2]. The shear strength of beams reinforced by fiber was calculated using hybrid support vector regression (SVR) and firefly optimization algorithm (FFA), and the designed model was shown to be robust in shear strength prediction [13]. ANN was integrated with the adaptive harmony search optimization (AHS) technique for modeling the shear strength of RC walls, and the proposed model accuracy was high [12]. Multivariate adaptive regression splines (MARS) and artificial bee colony (ABC) were also integrated to design a model for predicting the shear strength of RC deep beams, and the performance of MARS-ABC was higher than different building codes in shear strength estimation [16]. Generally, parameters of machine learning (ML) models are tuned using metaheuristic algorithms to improve the prediction efficiency of ML models [17–22].

Meanwhile, novel optimization algorithms have recently been developed, such as the African Vultures optimization algorithm (AVOA), particle swarm optimization (PSO), and Harris Hawks optimization (HHO). Although these techniques are used in different engineering applications [17–19], the AVOA optimization technique is not applied yet in shear strength prediction based on our literature. PSO was integrated with an adaptive neuro-fuzzy inference system (ANFIS) to predict the shear strength of high strength concrete for a slender beam, and the ANFIS-PSO attained the best modeling accuracy over ANFIS-ant colony optimizer (ANFIS-ACO), -differential evolution (ANFIS-DE), and -genetic algorithm (ANFIS-GA) [20]. Teaching-learning-based optimization (TLBO), PSO, and HHO were integrated with SVR, and the results of SVR-PSO, SVR-HHO, and SVR-TLBO were robust and can be used to estimate an accurate shear strength prediction of RC shear walls [21].

Based on the above literature, the hybrid SVR models are more robust for predicting the shear strength of RC deep beams [3,16,21,23]. This study aims to evaluate a new hybrid technique (SVR-AVOA) in predicting the shear strength of RC deep beams. To benchmark the proposed SVR-AVOA model, the hybrid known models SVR-PSO and SVR-HHO are proposed and compared; in addition, the recent mathematical studies and building codes are compared to the proposed model to assess its accuracy of it in modeling shear strength of RC beam. SVR-AVOA, SVR-PSO, and SVR-HHO are developed using different scenarios of input variables. For this study, 202 datasets, including 19 variables of experimental studies, were collected from literature to design and evaluate the proposed models. The sensitivity analysis of optimum input variables is proposed and evaluated.

2. Background of Variables Impacts the Shear Strength of RC Deep Beams

Figure 1i presents a real case of deep beam function in load transfer of buildings and variables that impact the shear strength value. Figure 1ii demonstrates the main parameters of the deep beam. Figure 1iii illustrates the failure mode of deep beams. In the figures, V represents the deep beam shear capacity, a is the horizontal distance from the load to the

support, and d denotes the deep beam depth. Here, V depends on (1) Concrete quality f'_c (for the diagonal strut), (2) Main steel yield strength f_y (for the main tie), and (3) Web reinforcement (horizontal and vertical). As some variables have a big role in forming the deep beam's shear strength, the main variables considered in this study are the shear span to depth ratio, the main reinforcement, ratio and yield strength, concrete compressive strength, and web reinforcement characteristics.

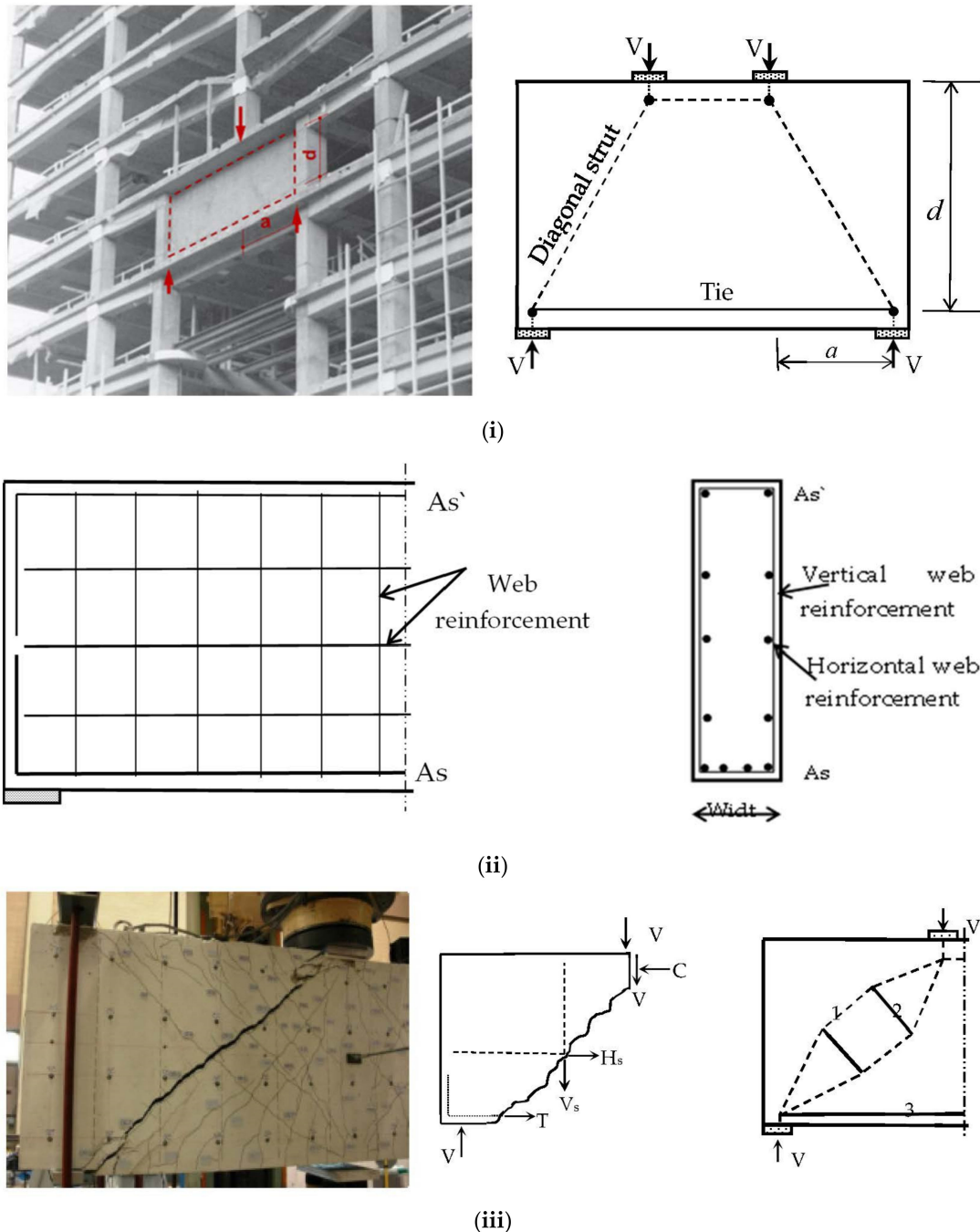


Figure 1. (i) Real case of using deep beams (left) and deep beam terminology (right); V : Shear strength, a : Shear span, d : Effective depth of beam. (ii) Basic reinforcement details of simple RC deep beam. (iii) Failure pattern in deep beam (left), Different mechanism components (middle), and Flow of forces in deep beam (right); where, C = compression force in concrete, T = tensile force in the main steel, H_s = tensile force in horizontal web reinforcement, V_s = tensile force in vertical web reinforcement; 1: Main diagonal strut, 2: Splitting tension force, 3: Main tensile force.

Many researchers investigated the deep beam's shear strength evaluation and predictions [1–4,24,25]. They concluded that the compressive strength of concrete (f'_c), the shear span to the beam's depth ratio (a/d), bottom longitudinal reinforcement ratio (ρ), and web reinforcement ratio (both vertical ρ_v and horizontal ρ_h) are the main key parameters. The previous analytical/experimental studies focused on the role of f'_c in forming V . In the case of beams with smaller a/d ratios, the role of the truss mechanism in transferring loads to the support location diminishes, and the direct diagonal strut is the main transferring load mechanism to the support's location. The effectiveness of such struts has a significant impact on V values [3]. Smith and Vantsiotis [26] and Ahmed [27] observed an increase in V of the deep beam with increasing f'_c of concrete, but the relationship was not linearly proportional. In addition, they observed no improvement in V if f'_c was above a certain limit. The non-proportional increase in shear strength compared to the increase in concrete compressive strength can be attributed to two reasons. First, the limited contribution of the aggregate interlock mechanism in members with high strength concrete compared to the one with normal strength concrete, as the cracks cross the aggregate particles in high strength concrete and do not go around them as in normal strength concrete. Second, the formed tensile strains perpendicular to the main diagonal strut work on reducing the benefits of using high strengths. Oh and Shin [28] noticed a brittle failure of deep beams with concrete of 74 MPa without any warning, which is different from the failure of other beams with 23 MPa. They also observed a decrease in the rate of increase in the ultimate strength of beams with high-strength concrete.

The inclination angle of the main diagonal strut plays a significant role in determining the concrete efficiency in the diagonal strut. This angle is directly dependent on the shear span to depth ratio a/d . As this angle increases, the forces can go directly inside the diagonal strut to the support. The previous studies [3,29] noticed that the increase in shear strength could be detected by decreasing the a/d ratio. Kim and Park [30] found a trivial impact of this ratio on the shear strength of beams with ratios greater than three, and the contrary was noticed for beams with ratios less than three. Oh and Shin [28] concluded that the ratio of a/d is the governing key parameter in determining the shear strength of a deep beam with high-strength concrete. In addition to resisting the induced tensile force of the main horizontal tie, the main reinforcement bars play an important role in controlling the width enlargement of the diagonal main cracks by dowel action mechanism and enable the aggregate interlock to work more effectively. Many researchers investigated the impact of the main reinforcement ratio on the deep beam's shear strength [3,31,32]. They observed a significant increase in the shear strength with increasing the main reinforcement ratio but up to a certain limit. Above a ratio of 1.5%, Ashour et al. [33] noticed a local concrete crushing damage due to compressive stress concentration at the top strut far from the main diagonal strut without enabling the diagonal strut to reach its ultimate resistance.

Web reinforcement has an important role in confining the concrete and delivering the tensile stresses at the main shear diagonal crack to the intact zones around the crack, which consequently increases the deep beam's shear strength [2]. Both vertical and horizontal web reinforcement has a key role in resisting shear stresses and limiting the enlargement of the width of the main diagonal crack [3]. In deep beams with higher a/d ratios, the contribution of vertical reinforcement is more obvious than the horizontal reinforcements, and the contrary is noticed for beams with a/d less than 1.0. As the deep beam's shear strength is dependent on many parameters, the increase of horizontal and vertical reinforcement above a certain limit does not influence the ultimate shear strength as other parameters may govern the situation without reaching the maximum capacity of the provided web reinforcement.

Table 1 presents the existing models used in this study compared to the developed models. The performance of these models was used significantly in shear strength determination for the RC deep beams of structures.

Table 1. Summary of existing models.

Ref.	Equation	Explanation
ACI [10]	$V_u = 0.17\sqrt{f'_c}bd + \frac{Avf_yd(\sin\theta + \cos\theta)}{s}$	θ is the angle between the stirrups and the beam longitudinal axis
Russo [8]	$V_u = 0.545 \left(kXf'_c \cos\alpha + 0.25\rho_h f_{yh} \cot\alpha + 0.35\frac{a}{d}\rho_v f_{yv} \right) bd$	$k = \sqrt{(n\rho)^2 + 2n\rho} - n\rho$ $\tan\alpha = \frac{a}{0.9d}$ $X = 0.74\left(\frac{f'_c}{105}\right)^3 - 1.28\left(\frac{f'_c}{105}\right)^2 + 0.22\left(\frac{f'_c}{105}\right) + 0.87$
Liu [4]	$V_u = V_{CLZ} + V_{ci} + V_s + V_d$	V_{CLZ} is the shear resisted at the critical loading zone, V_{ci} represents the contribution of aggregate interlock, V_s is the shear resisted by web reinforcement and V_d is the dowel action in the main longitudinal bars.

where: f'_c is the compressive strength of concrete, b is the beam width, d is the beam effective depth, Av is the vertical web reinforcement, f_{yv} and f_{yh} are the yield strength of vertical and horizontal web reinforcement respectively, s is the spacing between the vertical web reinforcement, ρ_h and ρ_v are the ratio of horizontal and vertical web reinforcement respectively, n is the modular ratio, ρ is the ratio of the main longitudinal bars.

3. Material and Data Collection

The Supplementary Material (Table S1) presents the data collected from the literature. For this study, 202 datasets were collected from the literature. In the current study, 19 input variables were used and divided into two categories, the main (8 variables) and other (11 variables) variables, as presented in Table S2. Here, the main variables were considered based on our literature in the previous section, Section 2; the other variables were considered while the impact on shear strength calculation was high. The direct relationship between each variable and the ultimate shear strength (V_u) of the RC deep beam is presented in Figure S1. Exponential, linear, logarithmic, and power functions were used to estimate the best direct relationship equation between V_u and input variables. Table 2 presents the summary of these functions.

Table 2. Direct relationship functions between V_u and input variables.

Variable	Equation (R^2)	Variable	Equation (R^2)	Variable	Equation (R^2)
a/d	$y = 358.43x^{-0.803}$ (0.26)	b	$y = 117.38 \times 10^{0.0052x}$ (0.21)	Ag	$y = 476.32x^{-0.164}$ (0.03)
ρ	$y = 65.95\ln(x) + 345.74$ (0.01)	d	$y = 0.7899x + 35.304$ (0.35)	Std	$y = 165.06 \times 10^{0.0731x}$ (0.05)
f_y	$y = 396\ln(x) - 2024.7$ (0.16)	h	$y = 0.6985x + 32.425$ (0.33)	Bd	$y = 524.3x^{-0.262}$ (0.03)
f'_c	$y = 495.94\ln(x) - 1234.7$ (0.39)	a	$y = 259.88 \times 10^{0.0003x}$ (0.015)		
ρ_v	$y = 325.96 \times 10^{-0.159x}$ (0.01)	Lp	$y = 169.42 \times 10^{0.0054x}$ (0.15)		
s	$y = 0.2678x + 344.21$ (0.06)	Sp	$y = 169.42 \times 10^{0.0054x}$ (0.15)		
f_{yv}	$y = 19.734x^{0.4588}$ (0.07)	V/P	$y = 199.58x + 199.66$ (0.010)		
ρ_h	$y = -371.18x + 429.11$ (0.10)	# bars	$y = 483.29\ln(x) - 199.43$ (0.37)		

where:
 y represents the V_u
 x represents input variables
 R^2 is the coefficient of determination

From Table 2, it can be observed that the power function has the best correlation with V_u in the case of using a/d and f_{yv} of the main variables. The relationship of ρ_v with V_u is exponential. The linear correlation can be detected between V_u and (s and ρ_h). ρ , f_y , and f'_c are correlated with V_u based on logarithmic functions. The best R^2 between V_u and the main variables is 0.39 for the f'_c variable. These results indicate that the relationship between the main variables and V_u cannot be estimated directly, and a complex relationship may be detected by using all main variables. Similarly, for the other variables, the relationship between V_u and variables varies. The best R^2 is estimated using a number of main bars, $R^2 = 0.37$. The variation in R^2 indicates the complex relationship between V_u and all variables. Table 2 and Figure S1 show the increase of the resistance

with beam effective width and height, number of main bars, and concrete strength up to a certain limit.

The statistical evaluation, range (RA), average (M), standard deviation (SD), kurtosis (KU), and skewness (SK) of the used datasets is presented in Table 3. From the table, the range of datasets varies and will affect the models' performances, so the normalized datasets are used to overcome the range change of variables. The data is normalized between 0 and 1 in this study. In addition, in the proposed models, it is recommended to use the given ranges of input variables. The average and standard deviation values show that the distortion of datasets is high. The kurtosis and skewness values indicate that the distribution of datasets is not normal. Figure 2 presents the histogram and distribution of main variables and V_u . The figure shows positive skewness for whole variables is observed; the distribution is also supported by the presented values in Table 3.

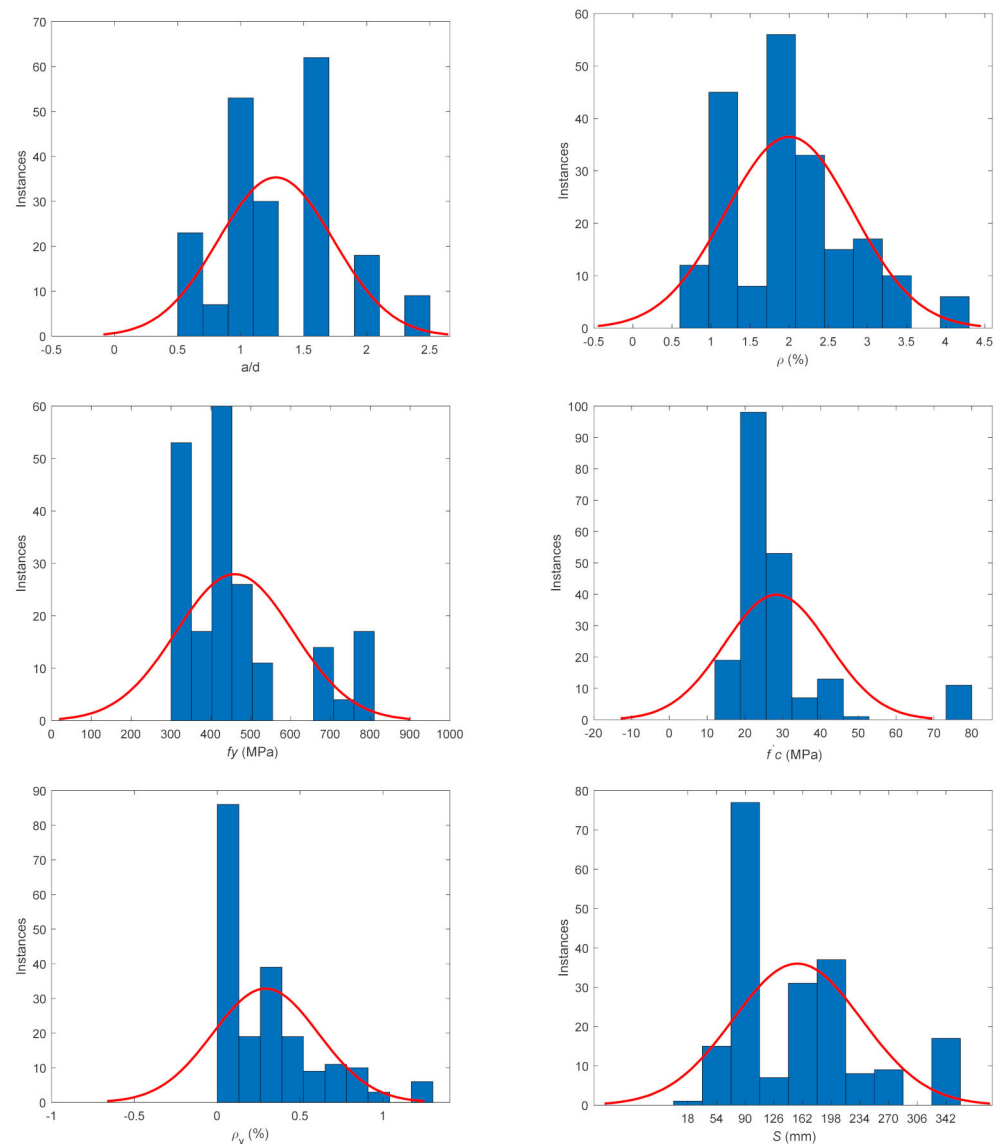


Figure 2. Cont.

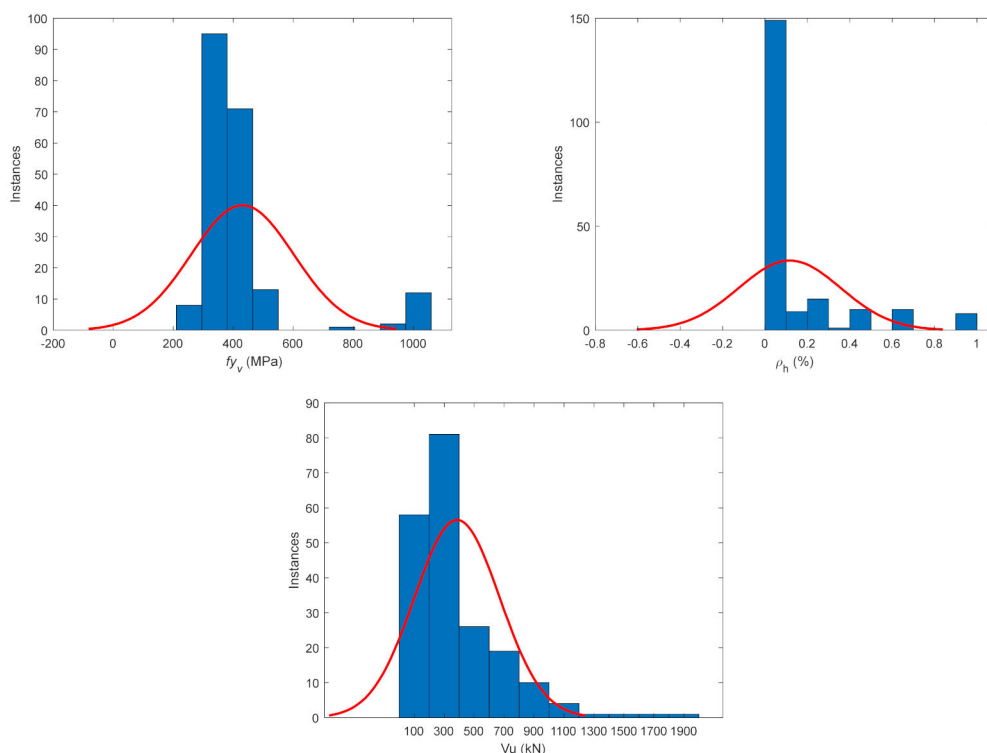


Figure 2. Distribution histogram of input and output variables.

Table 3. Statistical analysis of input and output variables.

Variable	RA	M	SD	KU	SK	Variable	RA	M	SD	KU	SK
a/d	1.93	1.28	0.46	−0.03	0.38	b (mm)	200.00	188.18	66.50	−0.94	0.28
ρ (%)	3.50	2.00	0.82	0.16	0.65	d (mm)	1374.00	443.74	212.19	11.52	3.14
f_y (MPa)	502.00	459.71	147.09	0.50	1.26	h (mm)	1550.00	505.91	235.73	12.91	3.32
f'_c (MPa)	66.10	28.33	13.75	7.04	2.64	a (mm)	1600.00	543.97	242.31	2.87	1.09
ρ_v (%)	1.25	0.29	0.32	0.69	1.10	L_p (mm)	210.00	113.11	45.63	3.05	2.04
s (mm)	330.00	155.33	80.63	0.54	1.07	S_p (mm)	210.00	113.11	45.63	3.05	2.04
f_{yv} (MPa)	791.00	430.68	171.05	6.12	2.55	V/P	0.50	0.93	0.16	2.96	−2.18
ρ_h (%)	0.91	0.12	0.24	3.58	2.15	#bars	10.00	3.61	1.70	10.50	2.95
V_u (kN)	1869.00	385.80	285.02	6.25	2.09	A_g (mm)	22.00	14.20	5.67	0.53	1.29
						Std (mm)	12.70	8.67	2.42	−0.38	−0.11
						Bd (mm)	6.20	7.66	2.08	−0.74	−0.65

4. Methods and Development Models

4.1. Support Vector Regression

Pal and Deswal [23] and Mozumder et al. [34] proposed the SVR formulas and theory in shear strength to predict RC beams. It was found to be a powerful computation technique for predicting the shear strength of deep beams [3,23]. Here, a summary of SVR is presented. SVR is the regression category of support vector machine (SVM), aiming to find a function that represents the relationship between inputs features to forecast the corresponding value when a new input is used. In SVR, “a fixed mapping procedure to map its input to n-dimensional feature space; then nonlinear functions are used to fit the high-dimensional features [35]”. Vapnik [35] proposed a loss function to allow the concept of SVM margin

to be used for regression solutions. The following equation represents the mathematical formula for the SVRs' approximation function [23,34]:

$$f(x) = w\varphi(x) + b \quad (1)$$

$$C = \frac{1}{2}w + C \frac{1}{n} \sum_{i=1}^n L(x, d) \quad (2)$$

where w and φ represent the weight vector and transformation functions, respectively; x and d are the input and output vectors, and b denotes a scalar. In Equation (1), the w and b are used to determine the normal and scalar vector, respectively, for the high-dimensional space, which is determined through $\varphi(x)$. Terms $\frac{1}{2}w$ and $C \frac{1}{n} \sum_{i=1}^n L(x, d)$ in Equation (2) are the standard error and the penalty terms, respectively. The ε -insensitive loss function introduced by Vapnik [34] is commonly used to estimate the Equation (1) parameters through the following minimization function [23,34]:

$$\text{minimize } 0.5 \|w\|^2 + C \sum_{i=1}^n (\zeta_i + \zeta_i^*) \quad \text{subjected to } \begin{cases} d_i - (wx_i) - b \leq \varepsilon + \zeta_i \\ (wx_i) + b - d_i \leq \varepsilon + \zeta_i^* \\ \zeta_i, \zeta_i^* \geq 0 \end{cases} \quad (3)$$

where $C > 0$, which controls the trade-off between the model complexity and the amount up to which deviations larger than ε are tolerated. Equation (3) can be transformed to a dual space using Lagrange multipliers solution. This solution can be expressed as follows [23,34]:

$$\text{maximize } L = -\varepsilon \sum_{i=1}^n (\alpha_i^* + \alpha_i) + \sum_{i=1}^n d_i (\alpha_i^* - \alpha_i) - 0.5 \sum_{i=1}^n \sum_{j=1}^n (\alpha_i^* - \alpha_i) (\alpha_j^* + \alpha_j) (x_i - x_j) \quad \text{subjected to } \begin{cases} \sum_{i=1}^n (\alpha_i - \alpha_i^*) = 0 \\ 0 \leq \alpha_i^* \leq C \\ 0 \leq \alpha_i \leq C \end{cases} \quad (4)$$

where L denotes the Lagrangian and α_i and α_i^* represent the Lagrange multiplier. Once Equation (4) is used to estimate the parameters of Equation (2), Equation (1) can be rewritten as [23,34]:

$$f(x) = \sum_{nsv} (\alpha_i^* - \alpha_i) (x_k \cdot x) + b \quad (5)$$

where nsv represents the number of support vectors (x_r, x_s). Here, the solution of this equation depends on the training pattern of Lagrange multipliers, which are only applied to estimate the w and b . Therefore, the kernel function is commonly used to solve the nonlinear regression problems in SVR. The Kernel functions can transform the nonlinear problems into linear problems, as presented in Yaseen et al. [36], which allows the SVR to solve more complex problems. The nonlinear SVR can be expressed as follows:

$$f(x) = \sum_{nsv} (\alpha_i^* - \alpha_i) K(x_i x) + b \quad (6)$$

where K is the kernel function; $K(x_i x) = (\varphi(x_i) \varphi(x))$. In the current study, the radial basis kernel (RBF) is applied.

It should be mentioned that the SVR is built with statistical theory and based on the minimization of structural risk principle [37]. It is a popular method for a small count of data, high dimensional, and non-linear problems. Therefore, SVR is used in many applications [13,38,39] for prediction tasks. Generally, SVR is a type of convex optimization technique to search a local solution within a problem domain [37]. The tuning of learning parameters of SVR greatly impacts the evaluation quality. Therefore, finding optimal values of SVR parameters from global searched cost is a difficult task [40]. Nature-inspired algorithms are proved to be successful in finding the local best solution from the global one.

This work applied and showed PSO, HHO, and AVOA for optimizing SVR parameters with faster convergence capability to provide better prediction accuracy of the SVR model in the deep beam's shear strength prediction.

4.2. Optimization Methods

To optimize the best parameters (C , ϵ , and KernelScale (γ)) of SVR, the PSO, HHO, and AVOA algorithms are used separately in the current work.

4.2.1. PSO

Kennedy and Eberhart (1995) proposed a metaheuristic population-based optimization algorithm named particle swarm optimization (PSO). The mechanism of the PSO is inspired by the fish schooling and foraging of the flock of birds while exploring an unknown region. Further, PSO is defined as a swarm of particles moving nearby the problem space by the influence of its global (G_{best}) and local best (P_{best}) position [41]. Therefore, a population search algorithm is used in PSO in a nature-inspired manner to analyze the input data features. The best position of the whole swarm is required to optimize the parameters. These can be performed through nature-inspired behaviors and learning experiences of population particles. PSO was found to be a robust integrated technique with SVR and ANN to model the shear strength of concrete [36,41,42]. PSO algorithm may be summarized as follows:

- First, it initializes the particle of the swarm, then defines the maximum number of iterations, and finally defines the cost function.
- After defining the cost function, it evaluates the swarm in order to identify the global and local best.
- Lastly, it calculates the velocity of each particle and then updates its position using the following equations:

$$v_{ik} = wv_{ik} + coef_1 rand_1 (P_{best,ik} - y_{ik}) + coef_2 rand_2 (G_{best,ik} - y_{ik}) \quad (7)$$

$$y_{ik} = y_{ik} + v_{ik} \quad (8)$$

where y_i denotes the i -th particle, k = the k -th dimension of the particle, $coef_1$ and $coef_2$ represent the acceleration coefficients, w refers to the inertia weight, $rand_1$ and $rand_2$ represent the random coefficients, which are randomly limited between zero and one. More details for PSO theory can be found in [43,44].

4.2.2. HHO

Heaidari and Mirjalili (2019) proposed a gradient-free, population-based optimization technique named Harris hawks optimization (HHO) [45]. The main inspiration behind HHO is surprised pounce, i.e., the chasing style and cooperative behavior of Harris' hawks in nature. According to the HHO optimization technique, numerous hawks cooperate to surprise a prey by pouncing it from multiple directions. They display a variety of pursuit patterns based on different scenarios and escaping patterns of the prey. The mechanism of HHO is that it mimics the Harris' hawk behavior in that trace, encircle, flush out, and attack the prey. It has been integrated with SVR and ANN to model the concrete characteristics and other engineering applications [21,46–49]. The main phases in the attacking of hawks are exploration (phase 1), transferring (phase 2), and exploitation (phase 3). In phase 1, the hawk depends on its position from the prey based on his waiting, seeking, and discovering; this can be expressed as follows:

$$Y(iter + 1) = \begin{cases} Y_{ranm}(iter) - r_1 | Y_{ranm}(iter) - 2r_2 Y_{ranm}(iter) & \text{if } n \geq 0.5 \\ (Y_{prey}(iter) - Y_m(iter)) - r_3 (LB + r_4 (UL - LL)) & \text{if } n < 0.5 \end{cases} \quad (9)$$

where Y_{ranm} and Y_{prey} indicate the random position for the selected hawk and prey's position, respectively. UL and LL indicate the upper and lower range; r_i indicates a random number, having a value between 0 and 1; and $Y_m = 1/N \sum_1^N Y_i(ite_r)$.

In phase 2, the prey energy is modeled as $E = 2E_0 \left(1 - \frac{ite_r}{T}\right)$, where T and $E_0 \in (-1, 1)$, and they indicate that energy falls for the prey with their escapes. Thus, the hawk can decide the solution based on the E computation and starting in phase 3 when $|E| \geq 1$, and exploiting the neighborhood when $|E| < 1$. Once starting phase 3, hawks decide to apply a soft or hard besiege. $|E| \geq 0.5$ indicates the prey still has enough energy to escape, but maybe some misleading jumps occur in it to fail, so a soft besiege works. On the other hand, in the case of $|E| < 0.5$, the prey is too fatigued to escape, so hard besiege works. Here, the HHO is used to optimize the SVR parameters.

4.2.3. AVOA

Abdollahzadeha and Gharehchopogh (2021) recently introduced a metaheuristic algorithm named African vultures' optimization algorithm (AVOA) [17]. The inspiration behind the development of the AVOA algorithm is the competing and searching behavior of vultures to acquire a large amount of food. To acquire a large amount of food, these vultures, ' N ' (N denotes the population of vulture), were divided into categories based on their fitness to find food and eat. The solution with the highest fitness value is treated as the first-best vulture and the second-best solution as the second-best vulture. The rest of the vultures were trying to approach the best vulture. This is formulated as follows.

Step 1: To determine the best vulture in the group. Fitness of all solutions is determined, and the best solution is selected as the best vulture of the group and other solutions will move towards the best solution using:

$$R(i) = \begin{cases} vulture_{best1} & \text{if } p_i = K_1 \\ vulture_{best2} & \text{if } p_i = K_2 \end{cases} \quad (10)$$

where the value of K_1 and K_2 lies between 0 and 1 with their sum equal to 1.

Step 2: Starvation rate of vultures. The starvation rate is the rate at which the vultures are satiated or hungry. The satiated rate has a declining trend, and to model, behavior Equation (11) is used,

$$F = (2ranm_1 + 1)P \left(1 - \frac{ite_r}{ite_{rmax}}\right) + t \quad (11)$$

$$t = h \left(\sin^w \left(0.5\pi \frac{ite_r}{ite_{rmax}}\right) + \cos \left(0.5\pi \frac{ite_r}{ite_{rmax}}\right) - 1 \right) \quad (12)$$

where F indicates the vultures are satiated. If the value of $|F|$ is greater than 1, vultures search for food in different areas, and the algorithm enters the exploration phase, whereas if the value is less than 1, AVOA enters the exploitation phase, and vultures search for food in the neighborhood. ite_r Indicates the iteration number, ite_{rmax} indicates the total number of iterations, $ranm_1$ has a random value between 0 and 1. Here, z and h indicate random numbers with values lying between -1 to 1 and -2 to 2 , respectively. If the value of z is less than 0, it indicates the vulture is starved, and if it increases to 0, it indicates the vulture is satiated. Here, w indicates the optimization operation disrupts the exploration and operation phases. By increasing the value of w , the probability of entering the exploration phase in the final optimization stages increases, and vice versa for decreasing the value of w .

Step 3: Exploration phase. In this phase, different random areas can be examined using two different strategies. To select the strategies in the $ranm_1$ exploration phase, a random number between 0 and 1 is generated. This procedure is shown in Equation (13).

$$P(i+1) = \begin{cases} R(i) - |XR(i) - P(i)|F & \text{if } P_1 \geq ranm_{P1} \\ R(i) - F + ranm_2((UB - LB)ranm_3 + LB) & \text{if } P_1 < ranm_{P1} \end{cases} \quad (13)$$

where $P(i + 1)$ indicates the vulture position vector in the next iteration, F indicates the rate of vulture being satiated, and $R(i)$ indicates one of the best vultures, which is selected at step 1 in the current iteration. X indicates a coefficient vector that increases the random motion by changing in each iteration and is obtained using the formula $X = 2 \times \text{ranm}$, where ranm is a random number between 0 and 1.

Step 4: Exploitation phase. In this phase, the efficiency stage of the algorithm is investigated. If the value of $|F|$ is less than 1, the algorithm enters the exploitation phase. Here, the exploitation phase is categorized based on the $|F|$ value. If $|F|$ is between 1 and 0.5, the rotating flight strategy of the vulture is processed based on parameter P_2 . This can be processed as follows:

$$P(i + 1) = \begin{cases} |XR(i) - P(i)|(F + \text{ranm}_4) - (R(i) - P(i)) & \text{if } P_2 \geq \text{ranm}_{P_2} \\ R(i) - \left[\left(R(i)(\cos(P(i))) \left(\frac{\text{ranm}_5 P(i)}{2\pi} \right) \right) + \left(R(i)(\sin(P(i))) \left(\frac{\text{ranm}_6 P(i)}{2\pi} \right) \right) \right] & \text{if } P_1 < \text{ranm}_{P_2} \end{cases} \quad (14)$$

If $|F|$ is less than 0.5, the two vultures' movements accumulate several types of vultures over the food sources, and the siege and aggressive strife to find food are implemented using parameter P_3 . This can be defined as follows:

$$P(i + 1) = \begin{cases} \frac{A_1 + A_2}{2} & \text{if } P_3 \geq \text{ranm}_{P_3} \\ R(i) - (|R(i) - P(i)|)(F)(LF(d)) & \text{if } P_3 < \text{ranm}_{P_3} \end{cases} \quad (15)$$

where,

$$A_1 = \text{vulture}_{\text{best1}}(i) - F \frac{\text{vulture}_{\text{best1}}(i)P(i)}{\text{vulture}_{\text{best1}}(i) - P(i)^2}; \text{ and } A_2 = \text{vulture}_{\text{best2}}(i) - F \frac{\text{vulture}_{\text{best2}}(i)P(i)}{\text{vulture}_{\text{best2}}(i) - P(i)^2} \quad (16)$$

$$LF(x) = 0.01 \frac{\mu\sigma}{|v|^{1/\beta}}, \quad \sigma = \left(\frac{\Gamma(1 + \beta) \sin(\pi\beta/2)}{\Gamma(1 + \beta^2)\beta 2((\beta - 1)/2)} \right)^{1/\beta} \quad (17)$$

In which, $\text{vulture}_{\text{best1}}(i)$ and $\text{vulture}_{\text{best2}}(i)$ are the best vulture of the first and second groups, respectively, in the iteration i ; d is the problem dimensions, μ and v denotes a random number between 0 and 1, and $\beta = 1.5$.

In this work, AVOA is used to tune the SVR parameter set to find the efficient performance of the SVR model.

4.3. Models' Development and Accuracy Assessment

This study proposed a new hybrid AVOA metaheuristic algorithm-based SVR model to find the optimal parameters (C , ε , and γ) of SVR and compare its performance with other two metaheuristics nature-inspired algorithms (called PSO and HHO)-based SVR model. Generally, the robustness of the SVR model depends on an appropriate selection of the parameters named as the penalty parameter/"BoxConstraint" (C), insensitive loss function/"epsilon" (ε), and the kernel parameter/"KernelScale" (γ/gamma). The range of these parameters is large, and it is difficult to search for the optimal set of values for these three parameters. Therefore, this optimization task may be solved using optimization algorithms. The authors of this article used three metaheuristic algorithms (AVOA, PSO, and HHO) to find the optimal parameter set of the SVR model. Figure 3 shows the process flow of the proposed technique. Initially, the missing value from the dataset is replaced using the k-nearest neighbor (KNN) imputer method. This study used a Euclidean distance measure to fill the missing value. The whole dataset is bifurcated into a train (80%) and test (20%) set. The three-metaheuristic algorithm is used to train SVR parameters for all/selected featured datasets separately. Root means squared error (RMSE) is selected as the fitness function of all algorithms. Metaheuristic algorithms are sensitive to their different parameter set. The Hit and trail approach is used to select the initial parameter set of metaheuristic algorithms. Table 4 shows the initial value of all parameters of three algorithms for SVR training. Since the number of epochs and population size affect the

convergence rate of metaheuristic algorithms, this research work aims to find a faster convergence rate of metaheuristic algorithm with 15 epochs and five population sizes (Table 4).

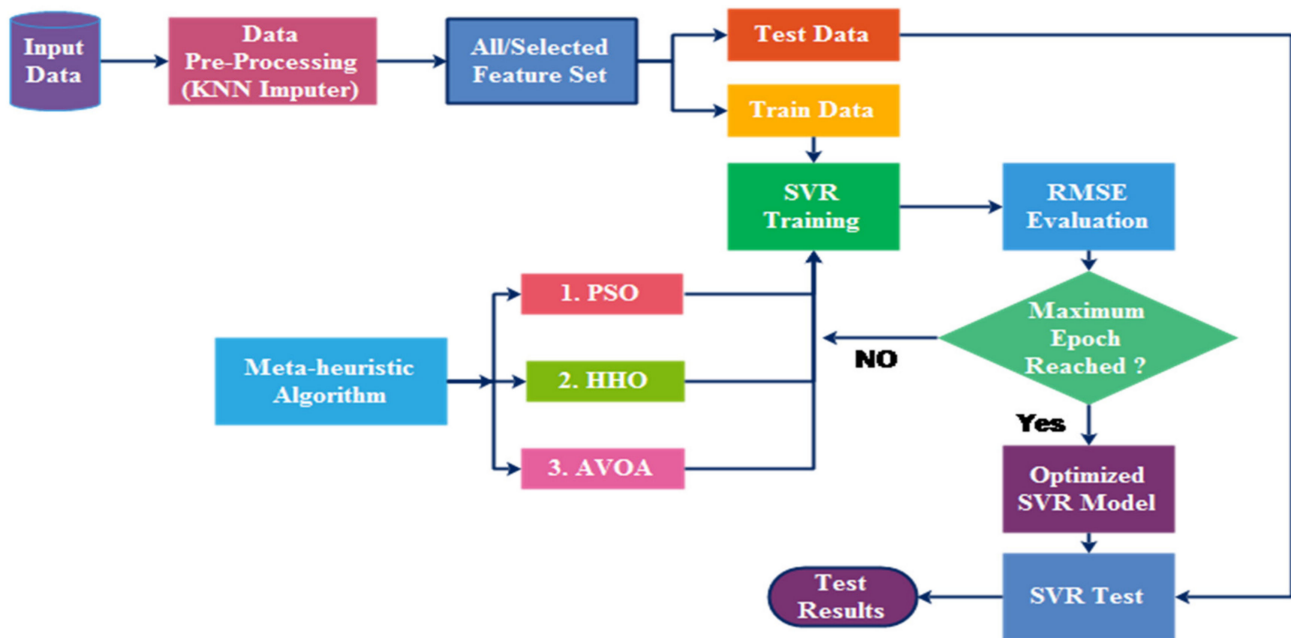


Figure 3. Process flowchart of the proposed method.

Table 4. Initial parameters of metaheuristic algorithms to train the SVR model.

Metaheuristic Algorithm	Parameters	Value
AVOA	Population	5
	Iteration	15
	P_1	0.9
	P_2	0.3
	P_3	0.6
	Alpha	0.8
	Beta	0.2
	Gamma	2.5
	Range of C	$[10^3, 10^{-3}]$
	Range of ϵ	$[10^3, 10^{-3}]$
Range of γ	$[10^3, 10^{-3}]$	
PSO	Population	5
	Iteration	15
	C_1	1
	C_2	2
	Range of C	$[10^3, 10^{-3}]$
	Range of ϵ	$[10^3, 10^{-3}]$
	Range of γ	$[10^3, 10^{-3}]$
HHO	Population	5
	Iteration	15
	N	3
	Range of C	$[10^3, 10^{-3}]$
	Range of ϵ	$[10^3, 10^{-3}]$
	Range of γ	$[10^3, 10^{-3}]$

To evaluate the accuracy of the proposed models, eight statistical indices are used: coefficient of determination (R^2), variance account factor (VAF), variance inflation factor (VIF), mean absolute error (MAE), root mean square error (RMSE), performance index (PI),

mean bias error (*MBE*), and percentage error (*PE*). The R^2 and *VAF* are used to measure the correlation between the measured and predicted values. *VIF* is used to evaluate the collinearity between the measured and predicted values; $VIF > 10$ indicates high collinearity. The models' errors are evaluated using *MAE*, *RMSE*, and *MBE*, and the *PE* is used to estimate the accuracy of the proposed model error in predicting the shear strength of RC deep beams. The mathematical expression of these indices can be expressed as follows:

$$R^2 = \frac{\sum_{i=1}^N (V_i - V_{mean})^2 - \sum_{i=1}^N (V_i - V_{pi})^2}{\sum_{i=1}^N (V_i - V_{mean})^2} \quad (18)$$

$$VAF = 100 \left(1 - \frac{var(V_i - V_{pi})}{var(V_i)} \right) \quad (19)$$

$$VIF = \frac{1}{1 - R^2} \quad (20)$$

$$RMSE = \sqrt{\frac{\sum_{i=1}^N (V_i - V_{pi})^2}{N}} \quad (21)$$

$$MAE = \frac{\sum_{i=1}^N |V_i - V_{pi}|}{N} \quad (22)$$

$$MBE = \frac{1}{N} \sum_{i=1}^N (V_i - V_{pi}) \quad (23)$$

$$PI = adj R^2 + (0.01VAF) - RMSE \quad (24)$$

$$PE = 100 \frac{RMSE}{V_{max} - V_{min}} \quad (25)$$

where V_i and V_{pi} represent the measured and predicted shear strength, V_{mean} , V_{max} , and V_{min} are the average, maximum, and minimum, respectively, of measured values, $adj R^2$ is the adjustment R^2 , and N is the number of the data sample.

4.4. Sensitivity Analysis

Cosine Amplitude Method (CAM) is used to analyze the strength of the relation between input the parameter and power factor [50]. It can also be used to determine the express similarity relation between correlated parameters. To apply CAM, all the data pairs were stated in common X -space. The data pairs used to construct a data array defined K as:

$$K = \{K_1, K_2, K_3, \dots, K_n\} \quad (26)$$

Every elements i.e., K_i , in the data array K is a vector of lengths j , i.e.,:

$$K_i = \{k_{i1}, k_{i2}, k_{i3}, \dots, k_{ij}\}_1 \quad (27)$$

Therefore, each of the data pairs is represented as a point in m -dimensional space, where each point requires j -coordinates for its complete description.

5. Results and Discussion

Two scenarios are presented in this section. The first is the evaluation of the proposed models based on all variables and the study of the effect of all variables on V_u estimation. Second, the main variables are considered in modeling and evaluating the sensitivity of

input variables on the best selection model. The best solution is compared to existing models in the shear strength determination of RC deep beams.

5.1. All Variables Impact on V_u Estimation

Table 5 presents the statistical indices of the proposed models. The numerical investigation of the statistical indices shows that the performance of the AVOA-SVR model is better to estimate V_u with $R^2 = 0.98$ and RMSE = 32.20 kN in the training stage. The comparison between all models using performance indices of all statistical indices in the training and testing stages shows that the AVOA-SVR model has a high index. However, the performance of HHO-SVR is better in terms of PI, RMSE, and PE in the testing stage. Moreover, Figure 4 illustrates the linear correlation between experimental and predicted V_u values for the proposed models. From Figure 4, it is shown that the performance of the AVOA-SVR model is more accurate than other proposed models in the training and testing stages. The distortion of data points around best fitting is small in modeling V_u with the AVOA-SVR model, and the VIF is higher than in other models, as presented in Table 5. This means that when we used all variables, the AVOA-SVR model can be used to estimate V_u with a model error approach of 6.95%.

Table 5. Statistical evaluation of the proposed models.

Training	R²	VAF	VIF	PI	RMSE	MAE	MBE	PE
AVOA-SVR	0.984	97.330	64.510	−30.241	32.198	24.377	−0.047	1.723
PSO-SVR	0.813	78.261	5.358	−89.973	91.568	31.605	26.960	4.899
HHO-SVR	0.818	66.278	5.500	−62.003	63.483	105.885	−6.032	3.397
Testing	R²	VAF	VIF	PI	RMSE	MAE	MBE	PE
AVOA-SVR	0.756	67.921	4.102	−76.076	77.505	101.702	−13.001	6.949
PSO-SVR	0.630	52.981	2.706	−75.687	76.837	106.357	17.850	6.889
HHO-SVR	0.715	45.786	3.514	−46.690	47.856	162.579	−56.320	4.290

The comparison between the AVOA-SVR model and previous studies is presented in Table 6. The statistical evaluation of relative predicted shear strength (V_u measured/predicted (V_m/p)) is presented in Table 6; COV is the coefficient of variation. From this table, it can be observed that the AVOA-SVR model performance is better and slightly better than ACI and Russo algorithms, respectively. Although the distortion around the mean for the proposed model is lower than for the Russo technique, the range of datasets for Russo is better than the proposed models. The Liu technique is better than previous and proposed models when considering the whole variables in modeling shear strength through the AVOA-SVR model. The selected variables are used and evaluated in the next section to estimate more accurate V_u values.

Table 6. V_m/p statistical evaluation for AVOA-SVR and previous studies.

Model	M	Maximum	Minimum	SD	COV
Liu [4]	1.10	1.54	0.65	0.15	0.13
Russo [8]	1.00	1.63	0.48	0.19	0.19
ACI [10]	0.59	2.06	0.09	0.41	0.69
AVOA-SVR	0.95	1.87	0.34	0.16	0.17

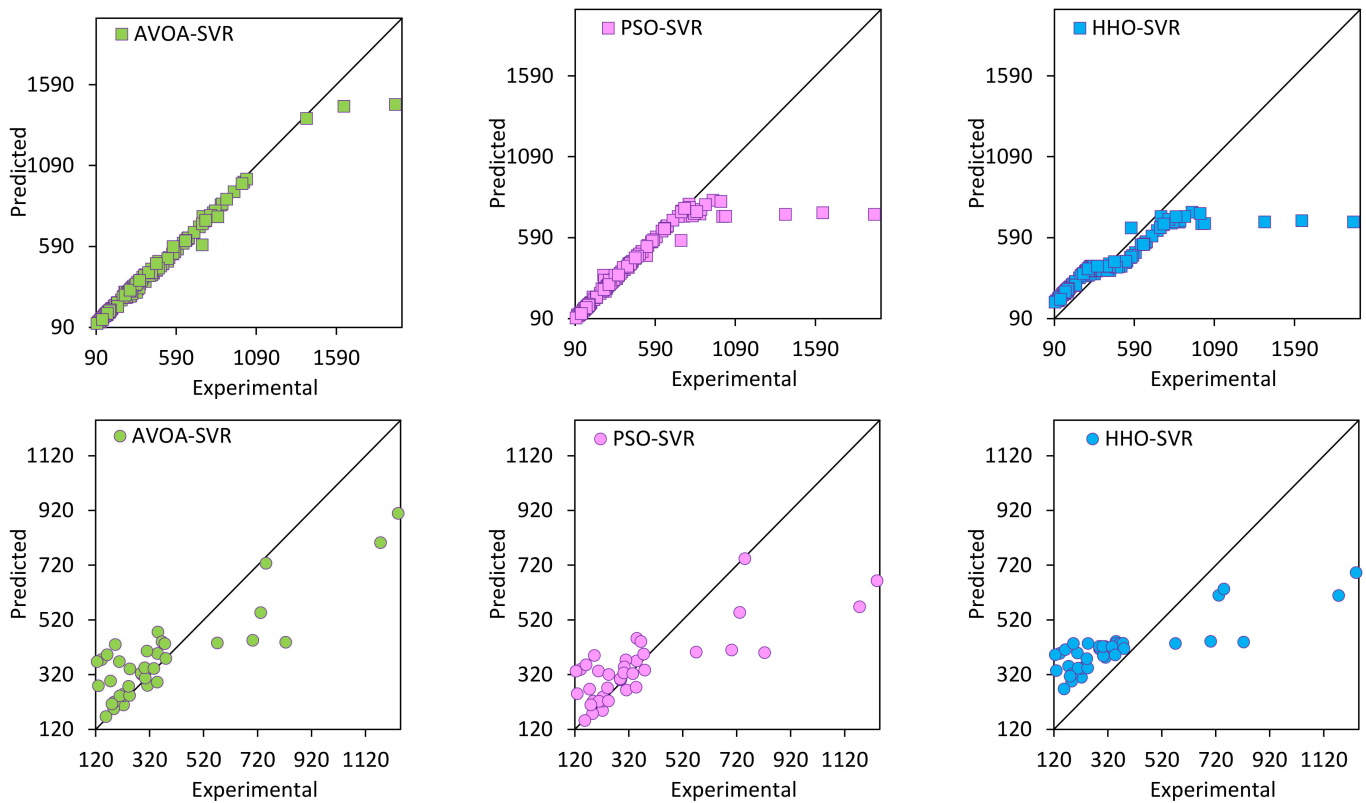


Figure 4. Scatter plot of model's performances in the training (**upper row**) and testing (**lower row**) stages.

5.2. Selected Variables Impact on V_u Estimation

Table 7 and Figure 5 present the performance evaluation of the proposed models. The performance of AVOA-SVR is high in the training stage. A high correlation, $R^2 = 0.97$, and low model error, $PE = 2.25\%$, are observed. In the testing stage, a low distortion around best fitting is observed with the AVOA-SVR. In addition, the statistical correlation factors are high, $R^2 = 0.97$ and $VAF = 94.46$, as presented in Table 7 and Figure 5. The VIF values of AVOA-SVR in the training and testing stages are higher than other models. This means the accuracy of AVOA-SVR is acceptable with low distortion around the observed values. Although the PI and RMSE of the HHO-SVR models are lower than for the AVOA-SVR model, the distortion of HHO-SVR datasets is high, as presented in Table 7 and Figure 5. Meanwhile, the performance of the proposed models is shown to be low to estimate the high shear strength (as presented in Figures 4 and 5). However, the performance of AVOA-SVR is seen as more robust. This indicates that AVOA-SVR can overcome the variation change in the data used. Figure 6 also shows a faster convergence rate of the AVOA-SVR model compared to the other two hybrid models. Therefore, the AVOA-SVR can be used to estimate the shear strength of RC deep beams with 3.4% model accuracy. The statistical comparison indices in Tables 5 and 7 show that the performance of proposed models with the selected variables is better than that for using all variables in modeling the proposed techniques. This means that the selected variables are more influential in the shear strength of RC deep beams.

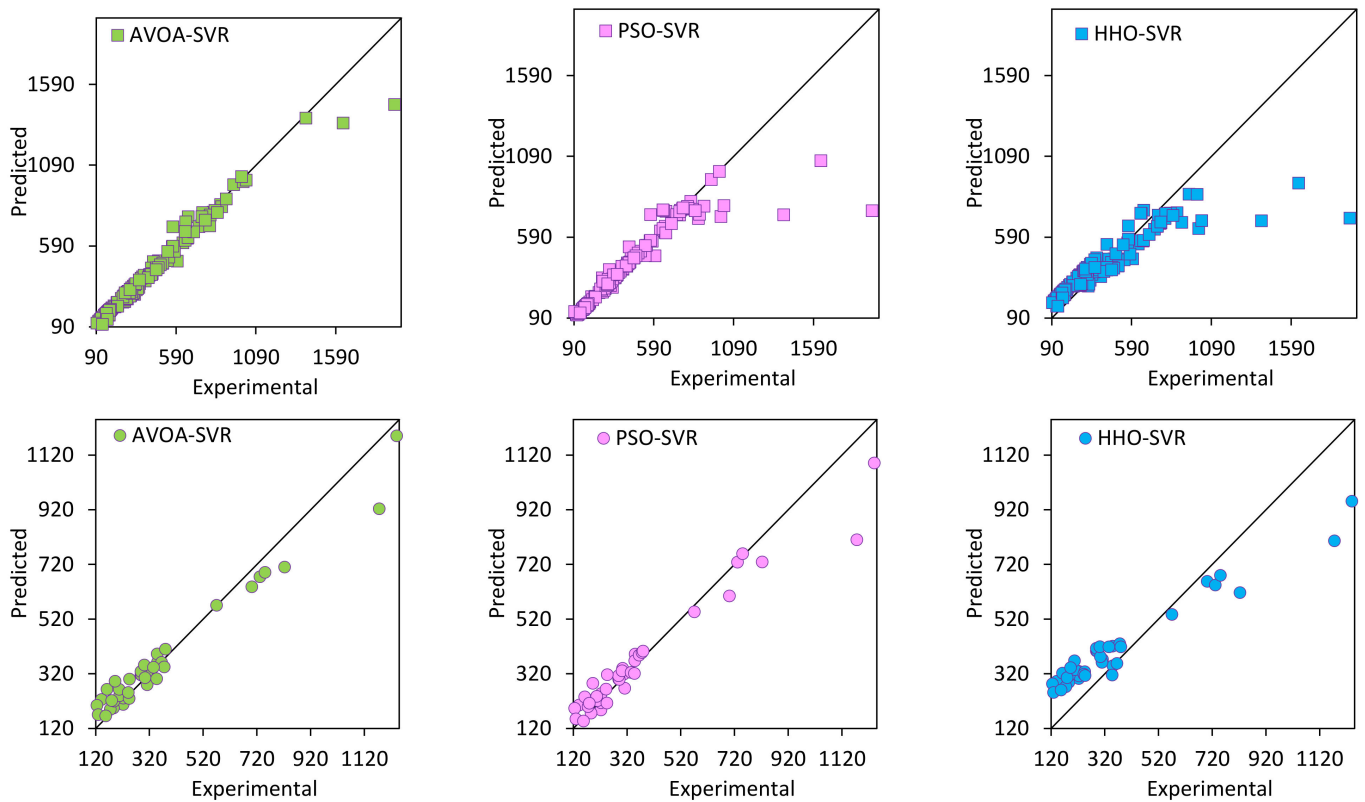


Figure 5. Scatter plot of model’s performances in the training (upper row) and testing (lower row) stages.

Table 7. Statistical evaluation of the proposed models.

Training	R ²	VAF	VIF	PI	RMSE	MAE	MBE	PE
AVOA-SVR	0.974	96.726	39.202	−40.095	42.036	26.728	−0.360	2.249
PSO-SVR	0.834	81.625	6.042	−90.753	92.402	32.755	18.958	4.944
HHO-SVR	0.816	71.805	5.427	−72.442	73.975	92.860	−7.926	3.958
Testing	R ²	VAF	VIF	PI	RMSE	MAE	MBE	PE
AVOA-SVR	0.970	94.460	33.512	−35.876	37.790	43.168	−7.149	3.388
PSO-SVR	0.950	91.774	20.118	−45.091	46.958	44.085	0.475	4.210
HHO-SVR	0.948	79.860	19.147	−33.841	35.586	106.952	−50.633	3.190

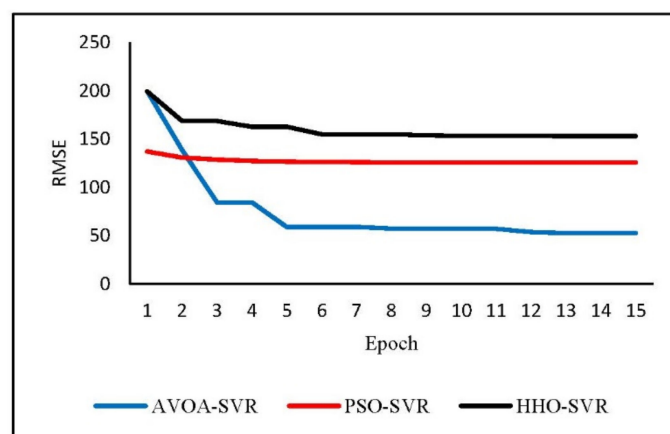


Figure 6. Convergence rate of three models.

5.3. Comparison with Previous Studies and Codes

Table 8 and Figure 7 show the performance of the proposed model compared to the previous studies' formulas. As seen in Table 8, the used selected variable improved the AVOA-SVR performance by 60% in terms of COV. This indicates that the selected variables are significantly affected by the V_u values of the RC deep beams. The comparison between previous formulas and AVOA-SVR shows that the proposed model accuracy is high in estimating the shear strength of RC deep beams. The small range is estimated with AVOA-SVR, and the range is 0.57 kN. The small SD and COV of the statistical indices are observed with AVOA-SVR. This means the accuracy of AVOA-SVR is high compared to other models.

Table 8. V_m/p statistical evaluation for AVOA-SVR and previous studies.

Model	M	Maximum	Minimum	SD	COV
Liu [4]	1.10	1.54	0.65	0.15	0.13
Russo [8]	1.00	1.63	0.48	0.19	0.19
ACI [10]	0.59	2.06	0.09	0.41	0.69
AVOA-SVR	0.98	1.33	0.76	0.07	0.07

The boxplot in Figure 7a shows that the median, red horizontal line of Russo, is close to the true value "1", followed by the AVOA-SVR and Liu models, respectively. The low interquartile range (IQR) value, the height of the box, is observed to be small with the AVOA-SVR model, followed by Liu and Russo models, respectively. The maximum and minimum quartiles, the black horizontal solid lines, are small with the AVOA-SVR model, followed by Liu and Russo models, respectively. The outliers are observed near the median of the AVOA-SVR and far to the median of the ACI model. From the visualization of boxplot results, it can be concluded that the performance of the AVOA-SVR model is more accurate than the previous studies for modeling the shear strength of RC deep beams. In addition, the following model is the Liu model, as this model considers more shear resistance mechanisms and shows a higher normal distribution and lower error than Russo's and ACI's models. The quantile-quantile (Q-Q) plot is presented in Figure 7b for the Liu and AVOA-SVR models for further investigation. The relative shear strength is presented versus the standard normal distribution. From this figure, both models have approximately followed the normal distribution; this indicates that both models can be used to estimate the shear strength of the RC deep beam. The AVOA-SVR model has more correlation with the standard normal distribution, and the AVOA-SVR model is more accurate than the Liu technique in modeling the shear strength of RC deep beams. The scatter plot presented in Figure 7c,d shows that the worst model for estimating the shear strength is the ACI's model. The variation in the best solution "1" is shown as small for Russo, Liu, and AVOA-SVR models, respectively. The most of relative shear strength of the AVOA-SVR model falls within $\pm 20\%$. The comparison of the AVOA-SVR model and previous models shows that the developed model can be used accurately to model the shear strength of the RC deep beams. Therefore, the AVOA-SVR model is a potential soft computing technique that can be used in predicting the shear strength of RC deep beams.

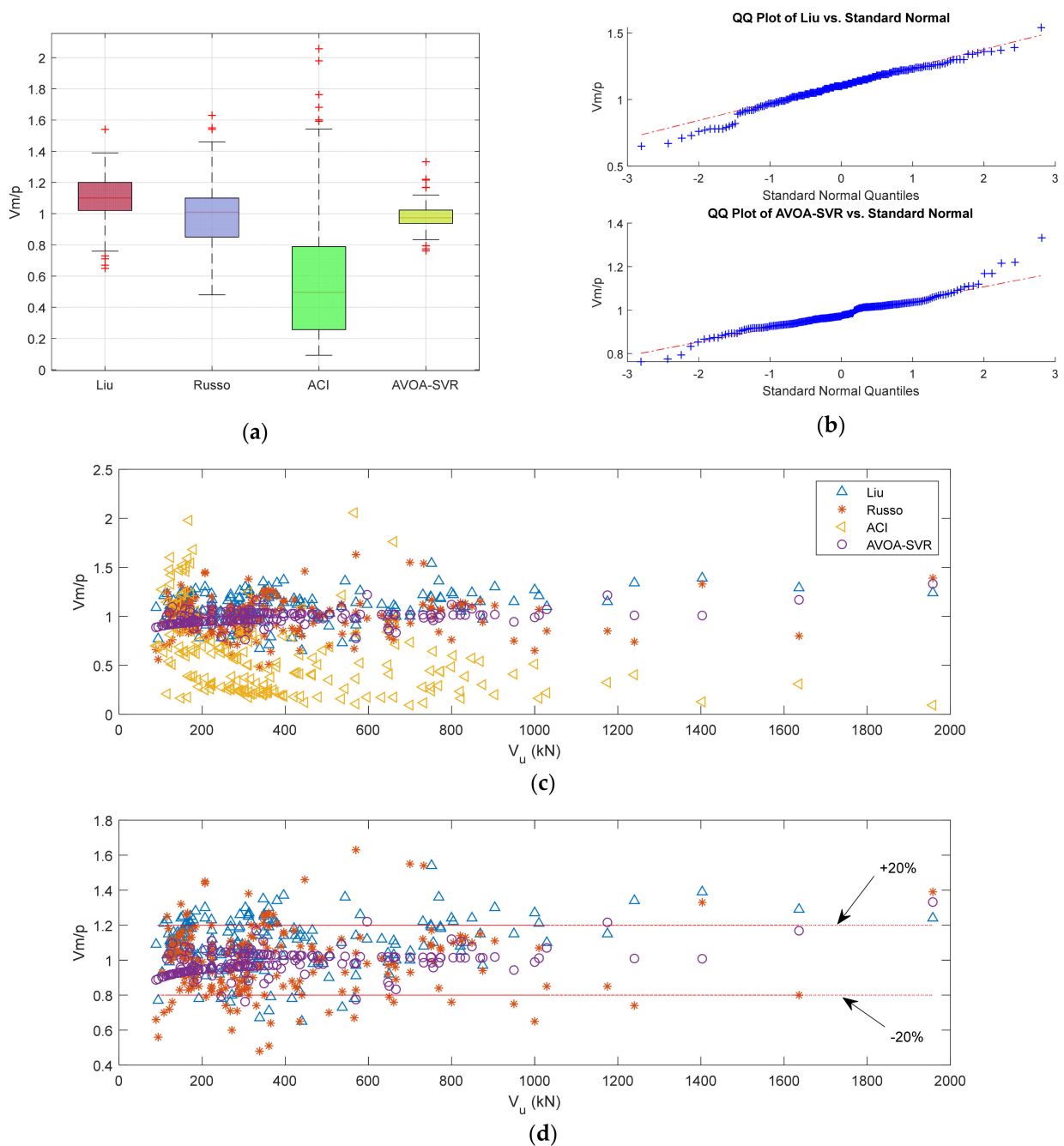


Figure 7. Comparison of model's performances, (a) boxplot, (b) Q-Q plot, (c) scatter plot of relative shear strength with measured shear strength, and (d) zoom in for upper plot with +20% limits for the best models.

5.4. Sensitivity Analysis of Input Variables

Figure 8 presents the most influential input variables in modeling the shear strength of the RC deep beam. The impact of the input variables is presented for the three models. From Figure 8, it can be noticed that the significant impact of the ratio of vertical and horizontal web reinforcements is low compared to other variables. The sensitivity of the shear span to depth ratio is high, followed by the yield strength of the main steel, the ratio of the main tensile bars, yield strength of vertical web reinforcement, stirrups spacing, and concrete compressive strength, respectively. The impact of the input variables on output for the other developed models is similar. These results imply that the shear strength of the RC deep beam is highly influenced by the beam geometry, concrete strength, and yield

strength of the steel bars. The stirrups spacing also has a large effect on the shear strength of RC deep beams.

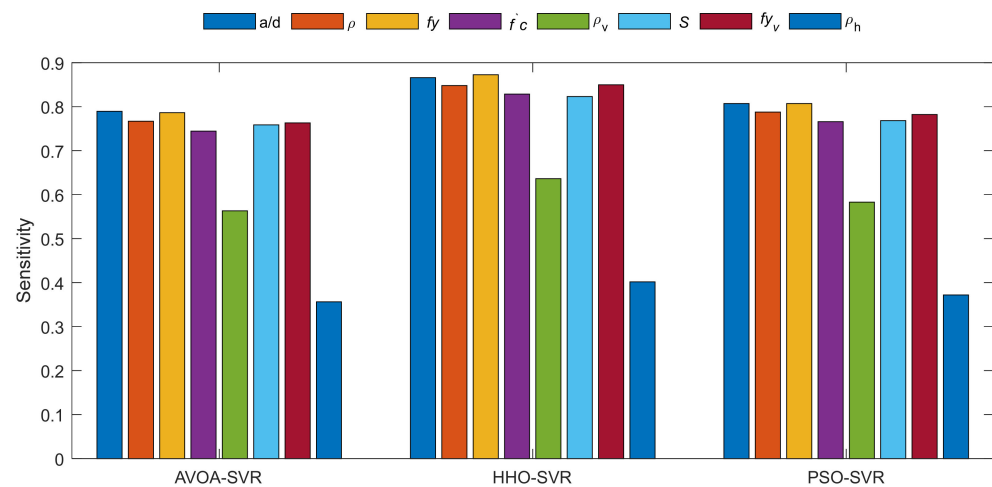


Figure 8. Sensitivity of input variable on model's prediction.

6. Conclusions

This study investigated the use of new metaheuristic optimization algorithms integrated with SVR to model the shear strength of RC deep beams and evaluate the sensitivity of input parameters. SVR-AVOA, -PSO, and -HHO were designed and compared to existing models in the current study. In this study, 202 datasets, including 19 variables of experimental studies, were collected from literature to design and evaluate the proposed models. The common eight parameters (shear span to depth ratio, the ratio of the main tensile bars, yield strength of main bars, concrete compressive strength, the ratio of vertical web reinforcement (stirrups), stirrups spacing, yield strength of vertical web reinforcement, and the ratio of horizontal web reinforcement) are also used to evaluate the performance of the proposed models' in predicting the shear strength of RC deep beams. The performance of SVR-AVOA is high in the cases of the used 19 and 8 parameters for modeling the shear strength. The accuracy of SVR-AVOA is improved by 60%, in COV terms, using the common input variables. Thus, other parameters were found less significant in modeling the shear strength of RC deep beams. The comparison of the SVR-AVOA and the previous studies shows that the accuracy of the proposed model is higher than Liu [4], Russo [8], and ACI [10] by 46%, 63%, and 90%, respectively, in terms of COV. This indicates that SVR-AVOA is the more robust model and can be accurately used in modeling the shear strength of RC deep beams. The sensitivity of the input variables in modeling the shear strength of RC beams with the SVR-AVOA was assessed. This investigation shows the impact of the shear span on the beam's depth ratio, yield strengths of vertical and horizontal web reinforcement, concrete compressive strength, stirrups spacing, and the ratio of the main longitudinal bars on the deep beams' shear strength.

Furthermore, the sensitivity of AVOA algorithm parameters can be tested to balance between exploitation and exploration side for enhancing the SVR performance. In the future, to check the efficiency of the proposed model should be tested on other datasets and other civil engineering application areas. The AVOA algorithm can be combined with other machine learning models like an extreme learning machine, random forest, etc., for prediction tasks.

Supplementary Materials: The following supporting information can be downloaded at: <https://www.mdpi.com/article/10.3390/su14095238/s1>, Figure S1: Direct relationship between inputs and output; Table S1: Data used in Modeling; Table S2: Modeling variables.

Author Contributions: Conceptualization, M.R.K. and B.S.A.; methodology, M.R.K. and B.R.; software, B.R.; validation, M.R.K., B.R. and B.S.A.; formal analysis, M.R.K. and B.S.A.; investigation, M.R.K., B.R. and B.S.A.; resources, B.S.A.; data curation, M.R.K. and B.S.A.; writing—original draft preparation, M.R.K., B.R. and B.S.A.; writing—review and editing, M.R.K., B.R., K.C. and B.S.A.; visualization, M.R.K., B.R., K.C., S.-M.K., H.-M.J. and B.S.A.; supervision, M.R.K. and J.-W.H.; project administration, M.R.K., J.-W.H. and B.S.A.; funding acquisition, J.-W.H. All authors have read and agreed to the published version of the manuscript.

Funding: This work was supported by Incheon National University Research Concentration Professors Grant in 2021.

Informed Consent Statement: Not applicable.

Data Availability Statement: The data used are available in the manuscript.

Conflicts of Interest: The authors declare no conflict of interest.

References

- Lee, Y.; Kim, S.; Kim, S. FEM Analysis of RC Deep Beam Depending on Shear-Span Ratio. *Archit. Res.* **2017**, *19*, 117–124.
- Gandomi, A.; Alavi, A.; Shadmehri, D.M.; Sahab, M. An empirical model for shear capacity of RC deep beams using genetic-simulated annealing. *Arch. Civ. Mech. Eng.* **2013**, *13*, 354–369. [[CrossRef](#)]
- Chou, J.-S.; Ngo, N.-T.; Pham, A.-D. Shear Strength Prediction in Reinforced Concrete Deep Beams Using Nature-Inspired Metaheuristic Support Vector Regression. *J. Comput. Civ. Eng.* **2016**, *30*, 04015002. [[CrossRef](#)]
- Liu, J. Kinematics-Based Modelling of Deep Transfer Girders in Reinforced Concrete Frame Structures. Ph.D. Thesis, Liege University, Liege, Belgium, 2019.
- Hwang, W.-Y.L.S.; Lee, H. Shear Strength Prediction for Deep Beams. *ACI Struct. J.* **2000**, *97*, 367–376. [[CrossRef](#)]
- Yavuz, G. Shear strength estimation of RC deep beams using the ANN and strut-and-tie approaches. *Struct. Eng. Mech.* **2016**, *57*, 657–680. [[CrossRef](#)]
- Nguyen, T.-A.; Ly, H.-B.; Mai, H.-V.T.; Tran, V.Q. On the Training Algorithms for Artificial Neural Network in Predicting the Shear Strength of Deep Beams. *Complexity* **2021**, *2021*, 5548988. [[CrossRef](#)]
- Russo, G.; Venir, R.; Pauletta, M. Reinforced Concrete Deep Beams-Shear Strength Model and Design Formula. *ACI Struct. J.* **2005**, *102*, 429–437.
- Dang, T.D.; Tran, D.T.; Nguyen-Minh, L.; Nassif, A.Y. Shear resistant capacity of steel fibres reinforced concrete deep beams: An experimental investigation and a new prediction model. *Structures* **2021**, *33*, 2284–2300. [[CrossRef](#)]
- ACI. *Building Code Requirement for Structural Concrete and Commentary*; ACI: Detroit, MI, USA, 2011; p. ACI-318.
- Ben Chaabene, W.; Nehdi, M.L. Novel soft computing hybrid model for predicting shear strength and failure mode of SFRC beams with superior accuracy. *Compos. Part C Open Access* **2020**, *3*, 100070. [[CrossRef](#)]
- Keshtegar, B.; Nehdi, M.L.; Kolahchi, R.; Trung, N.-T.; Bagheri, M. Novel hybrid machine learning model for predicting shear strength of reinforced concrete shear walls. *Eng. Comput.* **2021**, 0123456789. [[CrossRef](#)]
- Al-Musawi, A.; Alwanas, A.A.H.; Salih, S.; Ali, Z.; Tran, M.T.; Yaseen, Z.M. Shear strength of SFRCB without stirrups simulation: Implementation of hybrid artificial intelligence model. *Eng. Comput.* **2018**, *36*, 1–11. [[CrossRef](#)]
- Ning, C.; Li, B. Analytical probabilistic model for shear strength prediction of reinforced concrete beams without shear reinforcement. *Adv. Struct. Eng.* **2017**, *21*, 171–184. [[CrossRef](#)]
- Naderpour, H.; Nagai, K. Shear strength estimation of reinforced concrete beam–column sub-assemblages using multiple soft computing techniques. *Struct. Des. Tall Spéc. Build.* **2020**, *29*, 1–15. [[CrossRef](#)]
- Cheng, M.-Y.; Cao, M.-T. Evolutionary multivariate adaptive regression splines for estimating shear strength in reinforced-concrete deep beams. *Eng. Appl. Artif. Intell.* **2014**, *28*, 86–96. [[CrossRef](#)]
- Abdollahzadeh, B.; Gharehchopogh, F.S.; Mirjalili, S. African vultures optimization algorithm: A new nature-inspired metaheuristic algorithm for global optimization problems. *Comput. Ind. Eng.* **2021**, *158*, 107408. [[CrossRef](#)]
- Dragoi, E.N.; Dafinescu, V. Review of Metaheuristics Inspired from the Animal Kingdom. *Mathematics* **2021**, *9*, 2335. [[CrossRef](#)]
- Bagal, H.A.; Soltanabad, Y.N.; Dadjuo, M.; Wakil, K.; Zare, M.; Mohammed, A.S. SOFC model parameter identification by means of Modified African Vulture Optimization algorithm. *Energy Rep.* **2021**, *7*, 7251–7260. [[CrossRef](#)]
- Sharafati, A.; Haghbin, M.; Aldlemy, M.S.; Mussa, M.H.; Al Zand, A.W.; Ali, M.; Bhagat, S.K.; Al-Ansari, N.; Yaseen, Z.M. Development of Advanced Computer Aid Model for Shear Strength of Concrete Slender Beam Prediction. *Appl. Sci.* **2020**, *10*, 3811. [[CrossRef](#)]
- Parsa, P.; Naderpour, H. Shear strength estimation of reinforced concrete walls using support vector regression improved by Teaching–learning-based optimization, Particle Swarm optimization, and Harris Hawks Optimization algorithms. *J. Build. Eng.* **2021**, *44*, 102593. [[CrossRef](#)]
- Tosee, S.V.R.; Faridmehr, I.; Bedon, C.; Sadowski, Ł.; Aalimahmoudy, N.; Nikoo, M.; Nowobilski, T. Metaheuristic Prediction of the Compressive Strength of Environmentally Friendly Concrete Modified with Eggshell Powder Using the Hybrid ANN-SFL Optimization Algorithm. *Materials* **2021**, *14*, 6172. [[CrossRef](#)]

23. Pal, M.; Deswal, S. Support vector regression based shear strength modelling of deep beams. *Comput. Struct.* **2011**, *89*, 1430–1439. [[CrossRef](#)]
24. Zhang, D.; Shahin, M.; Yang, Y.; Liu, H.; Chang, L. Effect of microbially induced calcite precipitation treatment on the bonding properties of steel fiber in ultra-high performance concrete. *J. Build. Eng.* **2022**, *50*, 104132. [[CrossRef](#)]
25. Chen, B.; Zhou, J.; Zhang, D.; Su, J.; Nuti, C.; Sennah, K. Experimental study on shear performances of ultra-high performance concrete deep beams. *Structures* **2022**, *39*, 310–322. [[CrossRef](#)]
26. Smith, K.N.; Vantsiotis, A.S. Shear Strength of Deep Beams. *J. Am. Concr. Inst.* **1982**, *79*, 201–213. [[CrossRef](#)]
27. Ahmed, A.K.E.-S. Concrete Contribution to the Shear Resistance of FRP-Reinforced Concrete Beams. Ph.D. Thesis, University of Sherbrooke, Sherbrooke, QC, Canada, 2006.
28. Oh, J.-K.; Shin, S.-W. Shear Strength of Reinforced High-Strength Concrete Deep Beams. *ACI Struct. J.* **2001**, *98*, 164–173. [[CrossRef](#)]
29. El-Zoughiby, M.E. Z-Shaped Load Path: A Unifying Approach to Developing Strut-and-Tie Models. *ACI Struct. J.* **2021**, *118*, 35–48. [[CrossRef](#)]
30. Jin-Keun, K.; Yon-Dong, P. Shear strength of reinforced high strength concrete beam without web reinforcement. *Mag. Concr. Res.* **1994**, *46*, 7–16. [[CrossRef](#)]
31. Londhe, R. Shear strength analysis and prediction of reinforced concrete transfer beams in high-rise buildings. *Struct. Eng. Mech.* **2011**, *37*, 39–59. [[CrossRef](#)]
32. Mau, S.T.; Hsu, T. Formula for the Shear Strength of Deep Beams. *ACI Struct. J.* **1989**, *86*, 516–523. [[CrossRef](#)]
33. Ashour, A.; Alvarez, L.; Toropov, V. Empirical modelling of shear strength of RC deep beams by genetic programming. *Comput. Struct.* **2003**, *81*, 331–338. [[CrossRef](#)]
34. Mozumder, R.A.; Roy, B.; Laskar, A.I. Support Vector Regression Approach to Predict the Strength of FRP Confined Concrete. *Arab. J. Sci. Eng.* **2016**, *42*, 1129–1146. [[CrossRef](#)]
35. Vapnik, V. *The Nature of Statistical Learning Theory*; Springer: New York, NY, USA, 1995.
36. Yaseen, Z.M.; Tran, M.T.; Kim, S.; Bakhshpoori, T.; Deo, R. Shear strength prediction of steel fiber reinforced concrete beam using hybrid intelligence models: A new approach. *Eng. Struct.* **2018**, *177*, 244–255. [[CrossRef](#)]
37. Yap, C.W.; Li, Z.; Chen, Y. Quantitative structure–pharmacokinetic relationships for drug clearance by using statistical learning methods. *J. Mol. Graph. Model.* **2006**, *24*, 383–395. [[CrossRef](#)]
38. Du, K.; Liu, M.; Zhou, J.; Khandelwal, M. Investigating the Slurry Fluidity and Strength Characteristics of Cemented Backfill and Strength Prediction Models by Developing Hybrid GA-SVR and PSO-SVR. *Min. Met. Explor.* **2022**, *39*, 433–452. [[CrossRef](#)]
39. Liu, Q.; Li, S.; Yin, J.; Li, T.; Han, M. Simulation of mechanical behavior of carbonate gravel with hybrid PSO-SVR algorithm. *Mar. Georesour. Geotechnol.* **2022**, 1–14. [[CrossRef](#)]
40. Ortúzar, J. Future transportation: Sustainability, complexity and individualization of choices. *Commun. Transp. Res.* **2021**, *1*, 100010. [[CrossRef](#)]
41. Mohammed, A.; Kurda, R.; Armaghani, D.J.; Hasanipanah, M. Prediction of Compressive Strength of Concrete Modified with Fly Ash: Applications of Neuro-Swarm and Neuro-Imperialism Models. *Comput. Concr.* **2021**, *27*, 489–512.
42. Shahbazian, A.; Rabiefar, H.; Aminnejad, B. Shear Strength Determination in RC Beams Using ANN Trained with Tabu Search Training Algorithm. *Adv. Civ. Eng.* **2021**, *2021*, 1639214. [[CrossRef](#)]
43. Kennedy, J.; Eberhart, R. Particle Swarm Optimization. In Proceedings of the IEEE International Conference on Neural Networks, Perth, Australia, 27 November–1 December 1995; pp. 1942–1948. [[CrossRef](#)]
44. Yang, H.-C.; Zhang, S.-B.; Deng, K.-Z.; DU, P.-J. Research into a Feature Selection Method for Hyperspectral Imagery Using PSO and SVM. *J. China Univ. Min. Technol.* **2007**, *17*, 473–478. [[CrossRef](#)]
45. Heidari, A.A.; Mirjalili, S.; Faris, H.; Aljarah, I.; Mafarja, M.; Chen, H. Harris hawks optimization: Algorithm and applications. *Futur. Gener. Comput. Syst.* **2019**, *97*, 849–872. [[CrossRef](#)]
46. Golafshani, E.M.; Arashpour, M.; Behnood, A. Predicting the compressive strength of green concretes using Harris hawks optimization-based data-driven methods. *Constr. Build. Mater.* **2021**, *318*, 125944. [[CrossRef](#)]
47. Wei, W.; Li, X.; Liu, J.; Zhou, Y.; Li, L.; Zhou, J. Performance Evaluation of Hybrid WOA-SVR and HHO-SVR Models with Various Kernels to Predict Factor of Safety for Circular Failure Slope. *Appl. Sci.* **2021**, *11*, 1922. [[CrossRef](#)]
48. Zhang, H.; Nguyen, H.; Bui, X.-N.; Pradhan, B.; Asteris, P.G.; Costache, R.; Aryal, J. A generalized artificial intelligence model for estimating the friction angle of clays in evaluating slope stability using a deep neural network and Harris Hawks optimization algorithm. *Eng. Comput.* **2021**, 1–14. [[CrossRef](#)]
49. Sammen, S.; Ghorbani, M.; Malik, A.; Tikhamarine, Y.; AmirRahmani, M.; Al-Ansari, N.; Chau, K.-W. Enhanced Artificial Neural Network with Harris Hawks Optimization for Predicting Scour Depth Downstream of Ski-Jump Spillway. *Appl. Sci.* **2020**, *10*, 5160. [[CrossRef](#)]
50. Ji, X.; Liang, S.Y. Model-based sensitivity analysis of machining-induced residual stress under minimum quantity lubrication. *Proc. Inst. Mech. Eng. Part B J. Eng. Manuf.* **2015**, *231*, 1528–1541. [[CrossRef](#)]